A NEW APPROACH TO AUTOMATIC DISC LOCALIZATION IN CLINICAL LUMBAR MRI: COMBINING MACHINE LEARNING WITH HEURISTICS

Subarna Ghosh, Manavender R. Malgireddy, Vipin Chaudhary

Department of Computer Science and Engineering
State University of New York (SUNY) at Buffalo,
Buffalo, NY 14260

Gurmeet Dhillon, MD

Proscan Imaging Inc.
Williamsville, NY 14221

ABSTRACT

Lower back pain (LBP) is widely prevalent in people all over the world and negatively affects the quality of life due to chronic pain and change in posture. Automatic localization of intervertebral discs from lumbar MRI is the first step towards computer-aided diagnosis of lower back ailments. Till date, most of the research has been useful in determining a point within each lumbar disc, hence we go one step further and propose a localization method which outputs a tight bounding box for each disc. We use HOG (Histogram of Oriented Gradients) features along with SVM (Support Vector Machine) as classifier and successfully combine these machine learning techniques with heuristics to achieve 99% disc localization accuracy on 53 clinical cases (318 lumbar discs). We also devise our own metrics to evaluate the accuracy and tightness of our disc bounding box and compare our results with previous research.

Index Terms— Lumbar MRI, Automatic Disc Localization

1. INTRODUCTION

Lower back pain is the second most common neurological ailment in the United States after headache [1] with more than $50 billion spent annually on rehabilitation and healthcare. A matter of great concern is that, in the last decade there has been a severe shortage of radiologists [2] and by the year 2020 we expect a boom in the ratio of their demand and supply. This motivates us to automatically detect lumbar abnormalities from various scanning modalities to reduce the burden on radiologists and the average time for diagnosis.

Requirements for CAD systems of the lumbar region are unique since we need to localize and label the lumbar intervertebral discs before we can proceed to the important task of detecting abnormalities. Localization of lumbar discs is a challenging problem due to a wide range of variabilities in the size, shape, count and appearance of discs and vertebrae. To this end, we propose a robust method for labeling and localization of intervertebral discs in sagittal lumbar MRI images. The general flow of our approach is illustrated in Fig. 1. In the subsequent sections, we discuss in detail previous research (Sec. 2), our approach (Sec. 3) and experimental results (Sec. 4) and finally we draw our conclusion in Sec. 5.

2. PREVIOUS RESEARCH

There has been quite some research in the direction of localization of discs in lumbar MRI. Schmidt et al. [3] introduced a probabilistic inference method using a part-based model that measures the possible locations of the intervertebral discs in full back MRI. In [4], Bhole et al. presented a method for automatic detection of lumbar vertebrae and discs from clinical MRI by combining tissue property and geometric information from T1W sagittal, T2W sagittal and T2W axial modalities. They achieve 98.8% accuracy for disc labeling on 67 sagittal images. Alomari et al. [5] proposed a two-level probabilistic model that captures both pixel- and object-level features. The authors use generalized EM (Expectation Maximization) attaining an accuracy of 89.1% on 50 test cases. Oktay et al. [6] proposed another approach using PHOG (Pyramid Histogram of Oriented Gradients) based SVM and a probabilistic graphical model, and achieved 95% accuracy on 40 cases.

In previous research, authors have concentrated on finding a point inside the disc, which immediately leads to the added requirement of a challenging segmentation step in order to diagnose a disc abnormality. In our work we strive to provide tight bounding boxes for each disc in the lumbar region so that we can by-pass complicated segmentation algorithms and directly feed the detected disc region to a CAD system that extracts relevant features and automatically provides diagnostic results as detailed in our previous works [7, 8].

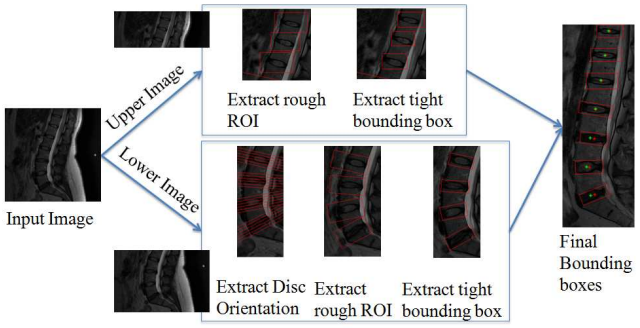

Fig. 1. This flow chart summarises the steps in our approach for disc localization in lumbar MRI. The 'lower' discs are those which have corresponding axial slices, and the rest of the visible discs are the 'upper discs'. The extraction of a rough ROI and finally the tight bounding box for each disc is detailed in Sec. 3.

3. PROPOSED APPROACH

3.1. Our clinical dataset

Clinical lumbar MRI used by our group is procured using a 3T Philips MRI scanner at Proscan Imaging Inc. It consists of manually co-registered T2 and T1 weighted sagittal views and T2 weighted

axial views. We randomly pick 53 anonymized cases, all of which have one or more lumbar disc abnormalities. According to the radiologist's report (which we treat as ground truth) there are a total of 65 herniated discs, 27 bulging discs, 26 desiccated discs, 60 degenerated discs and 73 discs having mild to severe stenosis. For our experiments we use T2 weighted mid-sagittal slice for each case. We use our own labeling tool for manual segmentation, which performs B-spline interplolation to interactively give a smooth outline of segmented regions. For our experiments, we get two sets of expert manual disc segmentation labeling all the visible discs starting from L5-S1 at the bottom. The dice coefficient is defined as : $Dice(A, B) = 2 * (A \cap B)/(A + B)$ where A and B are the two sets of disc pixels labeled manually. A mean dice coefficient of 0.88 for our dataset effectively illustrates the inter-observer variation.

3.2. Our Approach

Observing the clinical MRIs, we see that the technician acquires 6 axial slices for four or five lumbar inter-vertebral discs, changing the angle according to the orientation of the disc (Fig. 2(a)). Depending upon the case, axial views are recorded starting from L5-S1 and ending in either L2-L3 or L1-L2 giving rise to 24 or 30 axial slices.

In our approach for localization we find tight bounding boxes for all the visible discs (starting from L5-S1 and upwards) in the mid-sagittal MRI image for each case. We first localize the discs that have corresponding axial MRI by utilizing an approximate disc region calculated from the intersection of the axial slices with the sagittal as described in Sec. 3.4. Then we localize the remaining discs using a two stage classifier as detailed in Sec. 3.5. In both steps we use the HOG features as described in Sec. 3.3. From here on we will refer to the discs with corresponding axial slices as the 'lower discs' and the rest of the discs as the 'upper discs'.

3.3. HOG Feature Computation

Histogram of Oriented Gradients (HOG) are feature descriptors used in computer vision and image processing for the purpose of object detection [9]. This technique counts occurrences of gradient orientation in localized portions of an image. For our experiments, given a sub-image, we divide it into 3x3 = 9 sub-windows and fix the bin size to 9. Thus our HOG feature is a vector of length 81, which is the only feature we use for disc prediction.

3.4. Localization of Lower Discs

3.4.1. Extraction of rough bounding box

We first extract a rough inclined rectangular bounding box for each lower disc using the lines of intersection of the axial slices with the mid- sagittal slice (Fig. 2(a)). Then we empirically chop off $2/9th$ of the bounding box from the left and $3/9th$ from the right. Finally we locate the maximum intensity pixel (which corresponds to the spinal cord) and cut off some more on the right resulting in a better bounding box as illustrated in Fig. 2(b).

3.4.2. Creating the disc and non-disc training set

From the manual disc labels, we create 245 lower disc images (resized to 60x20) using the inclination of the axial slices. We also create around $15,000$ 60x20 non-disc images by sliding throughout the sagittal image. We divide the 53 cases (and hence the training disc and non-disc images) into fixed non-overlapping 10 folds to ensure that training and testing cases never intersect. We also make sure that these folds are fixed throughout our experiments.

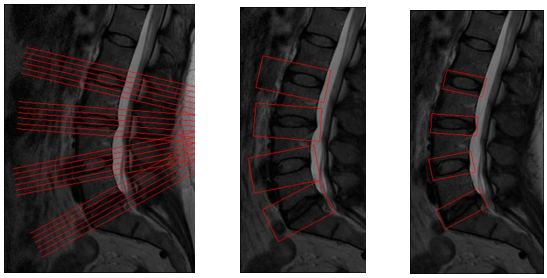

(a) (b) (c)

Fig. 2. Localization of the lower discs (Sec. 3.4) : (a) shows the lines of intersection of the mid-sagittal slice with all the available axial slices, (b) shows the rough lower disc ROIs extracted (Sec. 3.4.1), (c) shows the final bounding box for each lower disc as explained in Sec. 3.4.4.

3.4.3. SVM Training

We calculate HOG features (Sec. 3.3) for all the training images and model binary SVMs using libSVM [10] (a public implementation of Support Vector Machines for classification) for each fold (eg. for fold 1 we use the images in folds 2 to 10 and so on). Throughout the paper, our SVM classes are disc and non-disc, the kernel used is linear and we fix the best parameters by 5-fold cross validation within the training set.

3.4.4. Inclined Rectangular Tight Bounding Box

After obtaining the rough disc regions for each lower disc (Fig. 2(b)), we extract multi-scale and multi-aspect ratio rectangles by sliding throughout the rough ROI. Then we calculate HOG features for these rectangles which contribute to the test set for the lower discs. Using the SVM modeled in Sec. 3.4.3, we detect the top 20 candidate disc rectangles for each disc, and combine them by a weighted average to get the final tight bounding box as illustrated in Fig. 2(c).

3.5. Localization of the upper discs

3.5.1. Creating the disc and non-disc training set

Similar to Sec. 3.4.2, we create 166 disc images (resized to 80x40) using the manual labels of the upper discs, but this time the bounding boxes are not inclined since we do not have axial slice information for these discs. We also create approximately $10,000$ 80x40 non-disc images by sliding throughout the upper part of sagittal image (IsagUpper) decided by the upper-most axial line shown Fig. 3.

3.5.2. SVM training

Similar to Sec. 3.4.3 we train binary SVMs using HOG features from the upper disc training images.

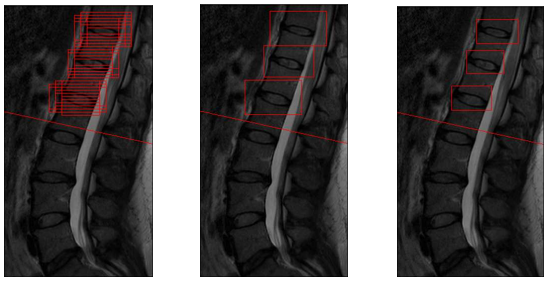

(a) (b) (c)

Fig. 3. Localization of upper discs (Sec. 3.5): In (a), (b) and (c), the inclined red line is the line of intersection with the uppermost axial slice, (a) shows the candidate disc rectangles, (b) shows the rough bounding boxes for the upper discs and (c) shows the final automatically detected bounding boxes for all the upper discs

3.5.3. Extraction of rough bounding box (Stage 1 classifier)

We extract multi-scale and multi-aspect ratio rectangles by sliding throughout IsagUpper and calculate corresponding HOG features. Using the trained SVM model (Sec. 3.5.2), we identify the disc rectangles (Fig 3(a)) and heuristically remove outliers by empirically deciding a deviation threshold on the centroid of the bounding boxes. We calculate the total number of upper visible discs (N_{upper}) from inter-disc distance of the lower discs localized in Sec. 3.4.4 and then cluster the disc rectangles into N_{upper} groups using the k-means algorithm. Finally, we combine rectangles in each group to give a rough bounding box for each upper disc (Fig 3(b)).

3.5.4. Rectangular Tight Bounding Box (Stage 2 classifier)

Stage 2 is the same as Sec. 3.4.4, with the only difference being that, the SVM model used is the one trained in Sec 3.5.2. This finally gives us the rectangular tight bounding box for each upper disc (Fig 3(c)).

4. EXPERIMENTAL RESULTS

4.1. Metrics

We calculate two commonly used metrics : 1) Deviation of disc centers (Dev_{eu}) is the euclidean distance (in mm) between the center of the automatically detected and that of the manual disc bounding box. 2) Accuracy(Acc) is the percentage of automatically detected disc centers which visually lie inside the disc.

We also devise our own metrics since our output is a tight bounding box and not just a point within the disc.

4.1.1. Deviation of Percent Disc pixels (DPD)

We define DPD as the deviation of the percentage of pixels in the manual bounding box belonging to disc(M_{per}) from the percentage of pixels in the automatic bounding box belonging to disc(A_{per}). We tabulate M_{per}, A_{per} and DPD to evaluate the tightness of the bounding box. Mathematically,

$$M_{per} = \frac{DiscPix_{manual}}{Pix_{manual}} * 100; A_{per} = \frac{DiscPix_{auto}}{Pix_{auto}} * 100 \quad (1)$$

where, $DiscPix_{manual}$ is the total number of disc pixels in the manual bounding box, Pix_{manual} is the total number of pixels in the manual bounding box, $DiscPix_{auto}$ is the total number of disc pixels in the automatic bounding box and Pix_{auto} is the total number of pixels in the automatic bounding box.

4.1.2. OutPercent (Out_{per})

Out_{per} is the percentage of disc pixels outside the automatic bounding box. It evaluates the accuracy of the bounding box.

$$Out_{per} = \frac{DiscPixOut_{auto}}{DiscPix_{manual}} * 100 \quad (2)$$

where $DiscPixOut_{auto}$ is the total number of disc pixels outside the automatic bounding box.

4.2. Results and Discussion

We perform 10-fold cross-validation on 53 cases and calculate performance metrics using two sets of manual segmentation as shown in Table 1. Note that the row 'Average' calculates the mean of the lumbar (L5-S1 to T12-L1) metrics whereas the row 'Upper' tabulates metrics of the upper discs which may contain one or more thoracic intervertebral discs. Even though we detect all the visible discs starting from L5-S1 and upwards, we tabulate the performance results separately for the six lumbar discs only, since they are the targeted ones in a lumbar MRI. From Table 1 we observe that the lower discs have tighter bounding boxes (lower DPD) than the upper ones, mainly because we don't have corresponding axial information for the upper discs. The upper bounding boxes, being less tight, also have lower Out_{per}. We achieve an average deviation of $1.59mm$ for the lumbar disc centers, which is better than the $3mm$ average distance reported in [6]. Also, we achieve an accuracy of 99% for correct localization of the lumbar disc centers. Fig. 4 shows some representative samples of our disc localization which prove the utility of our approach for a wide range of variabilities in the lumbar region.

Probabilistic graphical models [5] usually take a long time to train and converge. Our method uses simple HOG features with linear SVM which makes disc detection faster. Also, with the advent of GPUs and frameworks like CUDA, features from sliding windows can be calculated in parallel, potentially giving high detection speeds. Our method outputs a tight bounding box for each disc, hence, we eliminate intermediate error-introducing segmentation steps and can directly feed the bounding box for relevant feature extraction and abnormality detection [7, 8]. Unlike previous work [5, 6], this method can also handle variable number of discs in the lumbar MRI. Moreover, by using the axial slice information, we can consistently label the discs correctly, whereas in graphical models accurate labeling is challenging due to variabilities in the appearance of the L5-S1 disc.

5. CONCLUSION AND FUTURE WORK

We have proposed a new approach towards intervertebral disc localization from lumbar MRI: one that effectively combines machine learning with heuristics. We also move away from the general trend of simply finding a point within each disc, and instead output bounding boxes for each disc. Experiments on 53 clinical cases (some with extreme disorders) show encouraging results. We plan to experiment on larger datasets to localize discs using our approach in the immediate future. We also plan on using this approach to detect discs and

Table 1. Results : Automatic Disc Localization performance results using two sets of manual segmentation. The metrics are defined and explained in Sec. 4.1. Dev_{eu} is in mm and the rest are percentages.

Disc Label	Manual1 vs Auto					Manual2 vs Auto					
	M_{per}	A_{per}	DPD	Out_{per}	Dev_{eu}	M_{per}	A_{per}	DPD	Out_{per}	Dev_{eu}	Acc
L5-S1	54.08	54.43	-0.35	5.24	1.38	56.53	56.19	0.34	4.99	1.51	96.23
L4-L5	59.56	60.88	-1.33	6.74	1.45	60.19	62.22	-2.02	6.37	1.43	100.0
L3-L4	64.88	60.38	4.50	5.44	1.79	64.26	61.37	2.89	5.37	1.88	100.0
L2-L3	63.80	56.58	7.21	5.88	1.66	64.42	58.44	5.98	5.11	1.57	98.11
L1-L2	61.13	48.19	12.94	3.67	1.60	62.77	50.49	12.28	3.95	1.72	100.0
T12-L1	54.54	34.75	19.79	2.85	1.66	56.42	35.57	20.84	2.82	1.64	100.0
Average	59.66	52.54	7.13	4.97	1.59	60.77	54.05	6.72	4.77	1.63	99.06
Lower	60.92	57.45	3.46	5.81	1.60	61.85	59.20	2.66	5.48	1.64	98.68
Upper	54.70	34.79	19.91	3.29	1.79	56.76	36.22	21.54	2.98	1.78	98.11

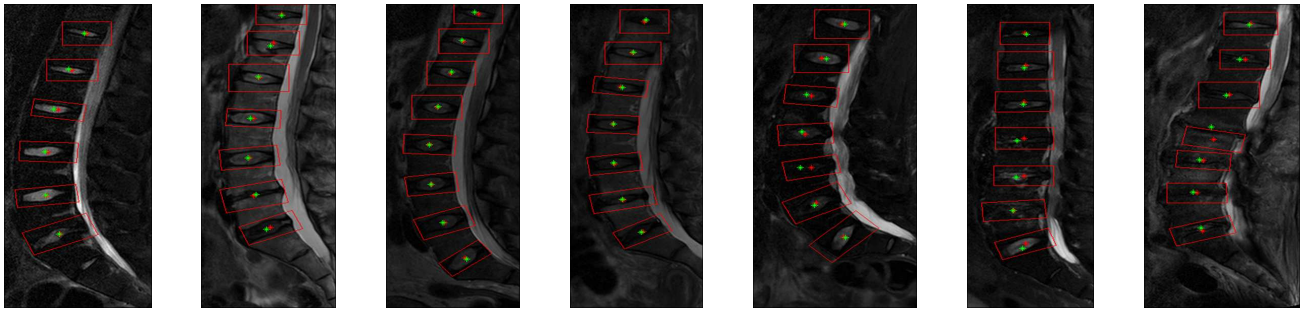

(a) (b) (c) (d) (e) (f) (g)

Fig. 4. Fully automatic disc localization - Red boxes are the automatic disc bounding boxes, red stars are the automatic disc centers and the green stars are the manual disc centers : (a), (b), (c) and (d) show correct bounding boxes and disc centers inspite of pathologies, (e) and (f) are extreme cases which show correct disc centers, (g) shows an extreme case where L2-L3 disc shows a wrong center and bounding box.

diagnose various disc abnormalities like herniation, desiccation and degeneration, to build a fully automatic and robust Lumbar CAD system.

6. REFERENCES

[1] D. K. Cherry, E. Hing, Woodwell, D. A., and E. A. Rechtsteiner, "National ambulatory medical care survey: 2006 summary," *National Health Statistics Reports*, vol. 3, pp. 1–39, 2008.

[2] M. Bhargavan, J. H. Sunshine, and B. Schepps, "Too few radiologists?," *American Journal of Roentgenology*, vol. 178(5), pp. 1075–1082, 2002.

[3] S. Schmidt, J. Kappes, V. Bergtholdt, M.and Pekar, S. Dries, D. Bystrov, and C. Schnoerr, "Spine detection and labeling using a parts-based graphical model," in *IPMI'07: Proceedings of the 20th international conference on Information processing in medical imaging*, 2007, vol. 4584, pp. 122–133.

[4] C. Bhole, S. Kompalli, and V. Chaudhary, "Context-sensitive labeling of spinal structures in mri images," in *The proceedings of SPIE medical imaging*, 2009.

[5] R.S. Alomari, J.J. Corso, and V. Chaudhary, "Labeling of lumbar discs using both pixel- and object-level features with a two-level probabilistic model," *Medical Imaging, IEEE Transactions on*, vol. 30, no. 1, pp. 1–10, 2011.

[6] Ayse Betül Oktay and Yusuf Sinan Akgul, "Localization of the lumbar discs using machine learning and exact probabilistic inference," in *MICCAI (3)*, 2011.

[7] S. Ghosh, R.S. Alomari, V. Chaudhary, and G. Dhillon, "Computer-aided diagnosis for lumbar mri using heterogeneous classifiers," in *Proceedings of the 8th IEEE International Symposium on Biomedical Imaging: From Nano to Macro,ISBI*, 2011, pp. 1179–1182.

[8] S. Ghosh, R.S. Alomari, V. Chaudhary, and G. Dhillon, "Composite features for automatic diagnosis of intervertebral disc herniation from lumbar mri," in *Engineering in Medicine and Biology Society,EMBC, 2011 Annual International Conference of the IEEE*, 2011, pp. 5068 –5071.

[9] N. Dalal and B. Triggs, "Histograms of oriented gradients for human detection," in *International Conference on Computer Vision & Pattern Recognition*, June 2005, vol. 2, pp. 886–893.

[10] Chih-Chung Chang and Chih-Jen Lin, *LIBSVM: a library for support vector machines*, 2001.